Solar Energy Materials & Solar Cells 248 (2022) 111964

Contents lists available at ScienceDirect

Solar Energy Materials and Solar Cells

journal homepage: www.elsevier.com/locate/solmat

Large grain size with reduced non-radiative recombination in potassium incorporated methylammonium-free perovskite solar cells

Gabriela S. Anaya Gonzalez [a,b,1], Jose J. Jeronimo-Rendon [c,1], Qiong Wang [a], Guixiang Li [a], Agustin O. Alvarez [e], Francisco Fabregat-Santiago [e], Hans Köbler [a], Alberto Alvarado [b], Hector Juárez-Santiesteban [b], Silver-Hamill Turren-Cruz [a,e,*], Michael Saliba [c,d], Antonio Abate [a]

[a] Department of Novel Materials and Interfaces for Photovoltaic Solar Cells, Helmholtz-Zentrum Berlin für Materialien und Energie, Kekuléstrasse 5, 12489, Berlin, Germany
[b] Benemérita Universidad Autónoma de Puebla. CIDS, Av. San Claudio y 18 Sur, Col. San Manuel, Ciudad Universitaria, CP 72570, P.O. Box 1067, Puebla, Pue, 7200, Mexico
[c] University of Stuttgart, Institute for Photovoltaics, Pfaffenwaldring 47, 70569, Stuttgart, Germany
[d] Helmholtz Young Investigator Group FRONTRUNNER, IEK5-Photovltaics Forschungszentrum Jülich, 52425, Jülich, Germany
[e] Institute of Advanced Materials (INAM), Universtitat Jaume I, Avda. V. Sos Baynat s/n, 12006, Castellón de la Plana, Spain

ARTICLE INFO

Keywords:
Perovskite solar cell
Photovoltaics
Potassium iodide

ABSTRACT

Organic–inorganic hybrid halide perovskites are widely considered to be one the most promising material in photovoltaic technology, the use of this semiconductor as absorbent layer in solar cells has attracted considerable interest due to their excellent properties. It has been reported that the incorporation of potassium ion is a powerful strategy to tune the perovskites properties, notwithstanding there has been some disagreement regarding the role of this monovalent alkali metal within the perovskite structure. Here, we investigated the impact of K^+ on the film properties and photovoltaic performance in double cation perovskite solar cells $Cs_{0.1}FA_{0.9}PbI_3$. Our results show that K^+ intervenes in the crystallization process inducing the extraction of non-reactive PbI_2 from the bulk, resulting in a notable enhancement in morphology and reduced non-radiative recombination. The solar cells fabricated with 3% of K^+ content achieve a PCE of 19.3%, showing a significative improvement in J_{sc}, V_{oc} and stability values compared with control devices.

1. Introduction

Organic-inorganic halide perovskites have been attracting considerable interest for over a decade; since their first appearance in 2009, there has been a rapid rise in using this novel material as a photo-active layer in solar cells [1,2]. Properties like a tunable bandgap, high defect tolerance, and long carrier diffusion length make this material suitable for optoelectronics and photovoltaics applications [3–5]. As a result of continuous research and engineering, perovskite solar cells performance (PSCs) has overtaken other photovoltaics technologies such as dye-sensitized, organic, CdTe, or CIGS-based solar cells, reaching more than 25% of power conversion efficiency (PCE) [6,7]. Despite the high efficiency and lower production cost compared with silicon solar cells, some constraints remain before industrialization can be achieved, e.g. toxicity, hysteresis, degradation, and instability [6,7].

Compositional engineering is an effective strategy to improve the properties of perovskite and suppress undesirable characteristics. In this regard, different approaches have been proposed. One of the most applied strategies is the cations mixing in the perovskite chemical formula ABX_3 where the A-cations methylammonium ($(CH_3NH_3)^+$, MA), formamidinium ($(CH_3(NH_2)_2^+$, FA) and Cs^+ have been extensively used. $MAPbI_3$ and $FAPbI_3$ were among the first perovskites used as a photo-active layer in solar cells and the most studied so far [8–11]. $MAPbI_3$ based solar cells have achieved high efficiencies but undergoing rapid decomposition when they are exposed to light or in dry air due to the volatile nature of MA [12]. On the other hand, $FAPbI_3$ can crystallize in the non-perovskite hexagonal phase δ-$FAPbI_3$, which does not have photo-active behavior. Nevertheless, FA-based perovskite generates

* Corresponding author. Department of Novel Materials and Interfaces for Photovoltaic Solar Cells, Helmholtz-Zentrum Berlin für Materialien und Energie, Kekuléstrasse 5, 12489, Berlin, Germany.
E-mail address: turren@uji.es (S.-H. Turren-Cruz).
[1] These authors contributed equally.

https://doi.org/10.1016/j.solmat.2022.111964
Received 13 May 2022; Received in revised form 16 August 2022; Accepted 20 August 2022
Available online 7 September 2022

considerable interest due to its wider bandgap and superior thermal stability compared to MA-based perovskites. Incorporating smaller cations such as Cs^+ and Rb^+ stabilize the α-$FAPbI_3$ cubic phase; the inorganic cations addition also enhance thermal and moisture stability [13]. In recent years, there has been growing interest in adding smaller alkali cations into perovskite to boost solar cells performance and enhance their stability [14–16]. In particular, potassium ion (K^+) has shown outstanding results tuning the properties of MAFA and CsMAFA perovskites [17,18]. Some researchers suggested that the enhancement exhibited after the addition of K^+ is due to the trapping defects reduction at the interface and ion migration suppression [19,20]. Studies on how the K^+ addition affects the device's performance have been carried out [21]. However, the role of this ion in solar cells properties and mechanisms is still being investigated; its location in perovskite lattice is still being discussed as well as its influence on the crystallization process.

Further work is therefore required, and a broader application of this cation on mixed perovskites is needed to elucidate its role and maximize the potential to modulate the properties of perovskite films and enhance the solar cell performance.

In this work, we examine and discuss the influence of K^+ on the morphological and electronic properties of $CsFAPbI_3$ perovskite. In previous works, we have shown that MA-free perovskites are promising materials due to their favorable bandgap and stability. Importantly, it appears that simple CsFA double cation perovskites suffer from an uncontrolled crystallization process with intermediate wide-bandgap contaminants that make reproducibility challenging to achieve. The addition of Rb, MA or Cs, respectively, has been shown to avoid this less controlled crystallization pathway. Thus, this triple cation approach appears to emerge as key for increased reproducibility [13,22,23].

In this context, we realize a triple cation composition by adding $KPbI_3$ solution into a $CsFAPbI_3$ perovskite precursor. The perovskite films $K_x(Cs_{0.1}FA_{0.9})_{1-x}PbI_3$ with ratios 0% (control film), 3%, 5% and 10% were obtained through one-step solution method. In addition, planar solar cells with structure Glass/ITO/SnO_2/Perovskite/Spiro-OMeTAD/Gold were fabricated to provide an experimental comparison from the photovoltaic behavior for solar cells with and without K^+.

Our results reveal that when the K^+ content is increased, perovskite grain size is notably enlarged which is associated to the XRD peaks, becoming more defined. This behavior suggests the PbI_2 by-product segregation from the perovskite film what eases the grain growth as we saw in SEM images. We also found that 3% K^+ concentration leads to a luminescence quantum yield of 0.65 and the highest PCE of 19.3% due to an enhancement in short circuit current and open-circuit voltage. Using impedance measurement, we extracted the characteristics values using an equivalent circuit from the two arcs spectra response, our results showed that V_{oc} follows the τ_{rec} response, reaching the highest value for the 3% K^+ device, this results means that at this concentrations more charge accumulation is achieved and as a consequence higher QFLS and V_{oc} values are reached.

2. Results and discussion

In this study, we investigated the effect of potassium content in the $CsFAPbI_3$ perovskite crystal structure. As it is further detailed in the experimental section, the perovskite film composition is figured as "$K_x(Cs_{0.1}FA_{0.9})_{1-x}PbI_3$", abbreviated for convenience as K_xCsFA where *x* is a percentage of KI added in the precursor solution. With our fabrication procedure that is detailed in the experimental section, we obtained devices with PCE approaching 20% with high reproducibility, as we report in this work.

Fig. 1 presents the XRD patterns from control, 3%, 5% and 10% K^+ films, this analysis runs in order to investigate the effect of potassium in the crystal structure of double cation perovskite. Observing the XRD film series we assure the formation of black phase perovskite, as it is seen on the characteristics peaks at 13.9° and 24.31° in 2 theta degrees, which is attributed to the (100) and (111) cubic phase planes [24]. In the other hand a strong intensity peak located at 12.7° is observed, which is assigned to PbI_2 compound, this is likely ascribed to the high temperature annealing (150 °C), necessary to get the black phase in FA-based perovskite[31]. This byproduct has an interesting XRD peak evolution, and its presence mainly affects the nature of crystallization and morphology. Here is clearly observed from the XRD patterns that K^+ has strong role on the film, promoting the crystallinity as it is observed in 3–10% perovskite peaks evolution. At the same time the K^+ ion promotes the PbI_2 ripening out from the grain boundaries resulting in PbI_2 peak intensity reduction as well as the formation of metallic like grains over the film observed in SEM images. The ripening effect can be explained with the formation of a K–Pb compound. Zooming the view of the XRD for small angles (Fig. 1B), two low-intensity peaks in 9.3° and 13.3° start growing at 3% K, increasing in intensity for larger concentration of K. These new XRD peaks could correspond to the potassium-rich phase K_2PbI_4 observed by Kuai [18], the low intensities presented by these peaks can be due to the small quantity of K^+ compared to the other elements presented in the film. Moreover, a shift

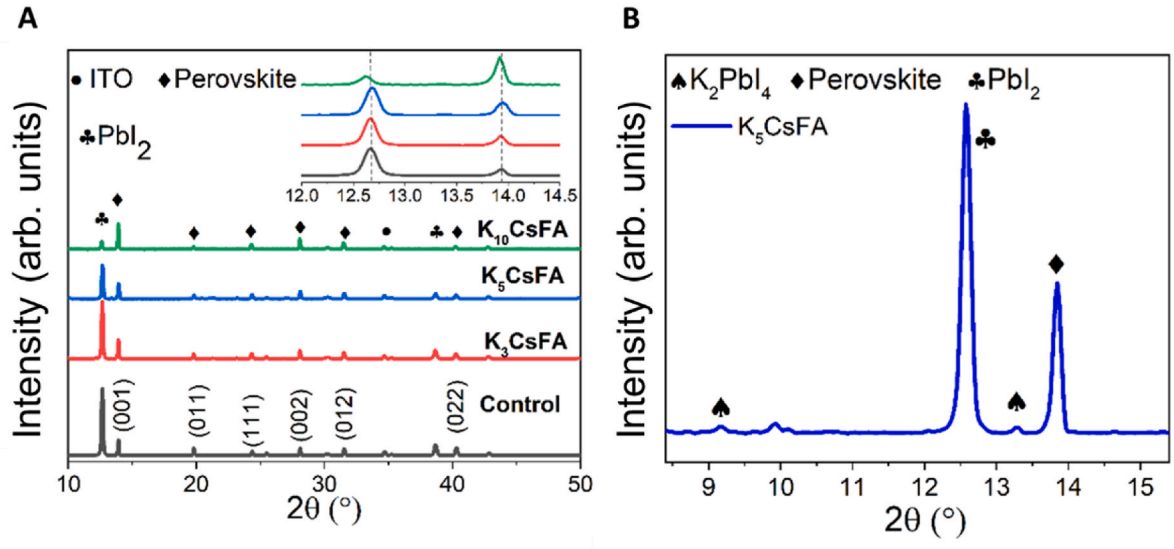

Fig. 1. A. XRD spectra for $K_x(Cs_{0.1}FA_{0.9})_{1-x}PbI_3$ series (Control and after addition of 3%, 5% and 10% of KI in the precursor solution). 1A Inset image on top, **B.** XRD spectra for low intensity peaks (took it from Fig. 1A).

in the XRD peaks to lower angles is observed in Fig. 1B, this shift has been observed in previous findings and it is ascribed to a slight change of iodide-bromide ratio, which induces the lattice expansion. In this work pure iodine perovskites are studied, then we associate the shift to lower angles to K_2PbI_4 molecules trapped in the perovskite lattice, generating a structure distortion. This result does not contradict the previous reported research, where it is established that K^+ by itself is not occupying a site in the ABX_3 structure [21,25], since we are proposing the insertion of a K_2PbI_4 molecule in the material rather than the formation of a $KPbI_3$ perovskite or K^+ taking substitutional sites.

From the SEM images in Fig. 2(A-D), it is observed that there is a difference between crystallite size and homogenization. Taking the data from the control sample, there is no uniformity in grain size distribution, which goes from a hundred nanometers to 3 or 4 times that value as it is observed in Fig. S1. Additionally, a huge dispersion of brighter grains over the perovskite film is observed that could be due to the PbI_2 metallic like formation, matching the XRD pattern. These particles are growth/crystallized mainly in the grain perovskite boundaries, this could explain the intense peak in the corresponding XRD pattern (see Fig. 1 control pattern). As 3% of K^+ content is added, morphological changes are observed, such as an increase in perovskite grain size and the amount of metallic-like particles, which could be the ripening of PbI_2 promoted by the monovalent ion. The role played by the K ion could be as an agent that surrounds the perovskite and do not allow the PbI_2 deposition, probably by suppressing the diffusion of PbI_2 into the film. It is also observed that some PbI_2 grains start to coalescence during the crystallization process, this uptake of PbI_2 is in agreement with the XRD results. When the K^+ concentration is raised to 5% the coalescence effect starts governing the metallic like grains letting them grow bigger, simultaneously the perovskite film surface is affected, observing a grain growth and a quasi-homogeneous film that exhibit an average grain size of 600 nm. This monovalent ion not only contributes to the byproduct uptake also subserves the perovskite crystallization as this is observed when the K^+ concentration is 10% obtaining a 800 nm perovskite grains in average, and PbI_2 coalescence of 300 nm in size. So according to the X-ray data and the present SEM images; it can be suggested that the PbI_2 peak intensity is almost diminished when the perovskite solution is saturated with K ion segregating this compound towards perovskite film surface. The domains associated to PbI_2 compound are only observed at the SEM images surface, and no were detected on the transversal images analysis (metallic-like grains), this could confirm that the PbI_2 byproduct is only formed on the perovskite film surface due to the effect of K incorporation.

EDX mapping of K_xCsFA samples is presented in Fig. 3. The EDX analysis was measured on the white and black particles. Those particles we selected explicitly, as we can see in Fig. 3B, and S2. EDX spectra have confirmed the presence of elements such as potassium (K), lead (Pb), iodide (I), and cesium (Cs), which corresponds to the perovskite material presented in this work. From the EDX mapping we confirm that K^+ is not occupying a site within the perovskite structure, since we did not find any content of this metal in the grains associated to perovskite material, nevertheless small K^+ signal was found in the white dots, as expected

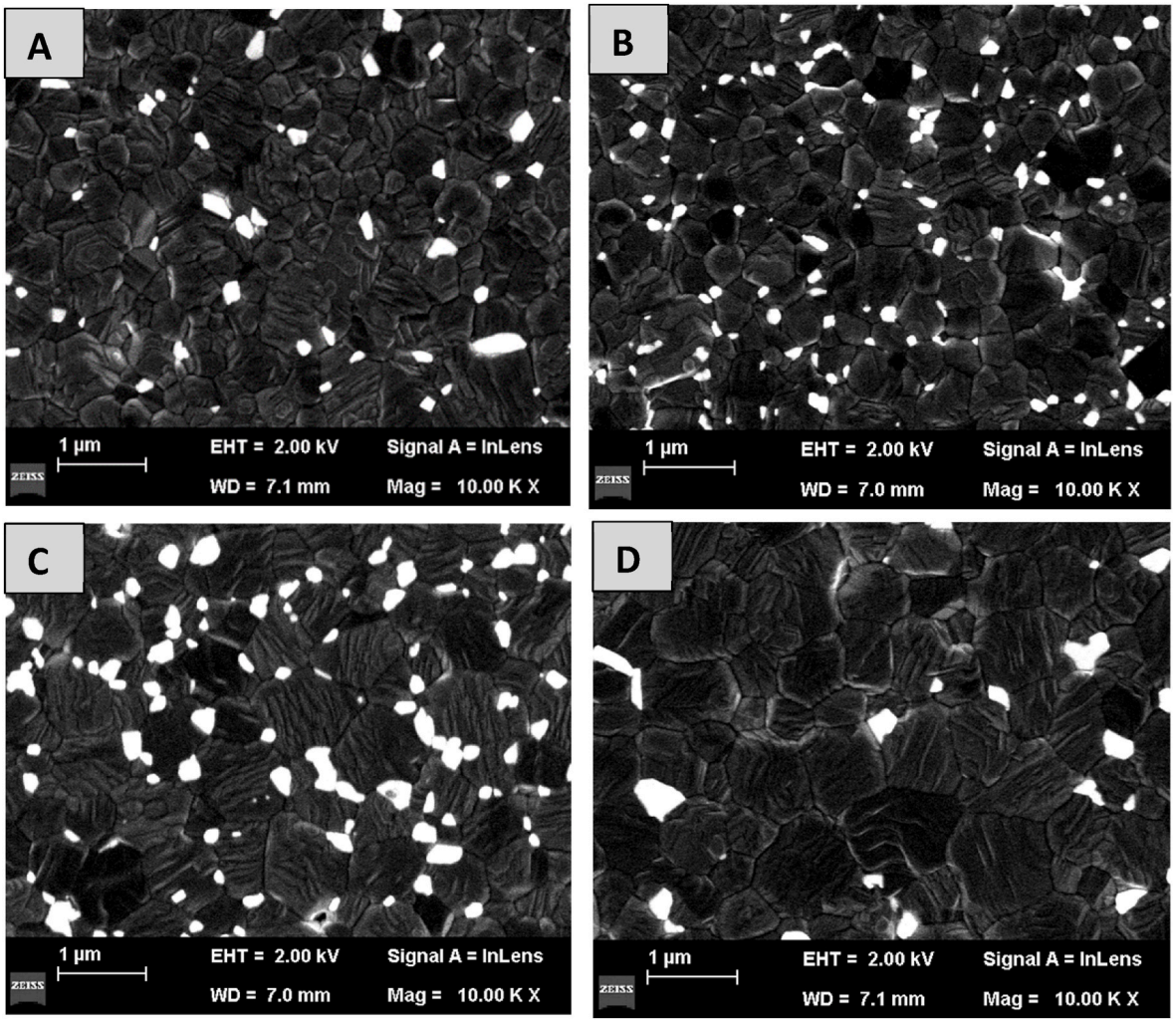

Fig. 2. Top-view SEM images of samples A. Control film, B. K_3CsFA, C. K_5CsFA, and D. $K_{10}CsFA$.

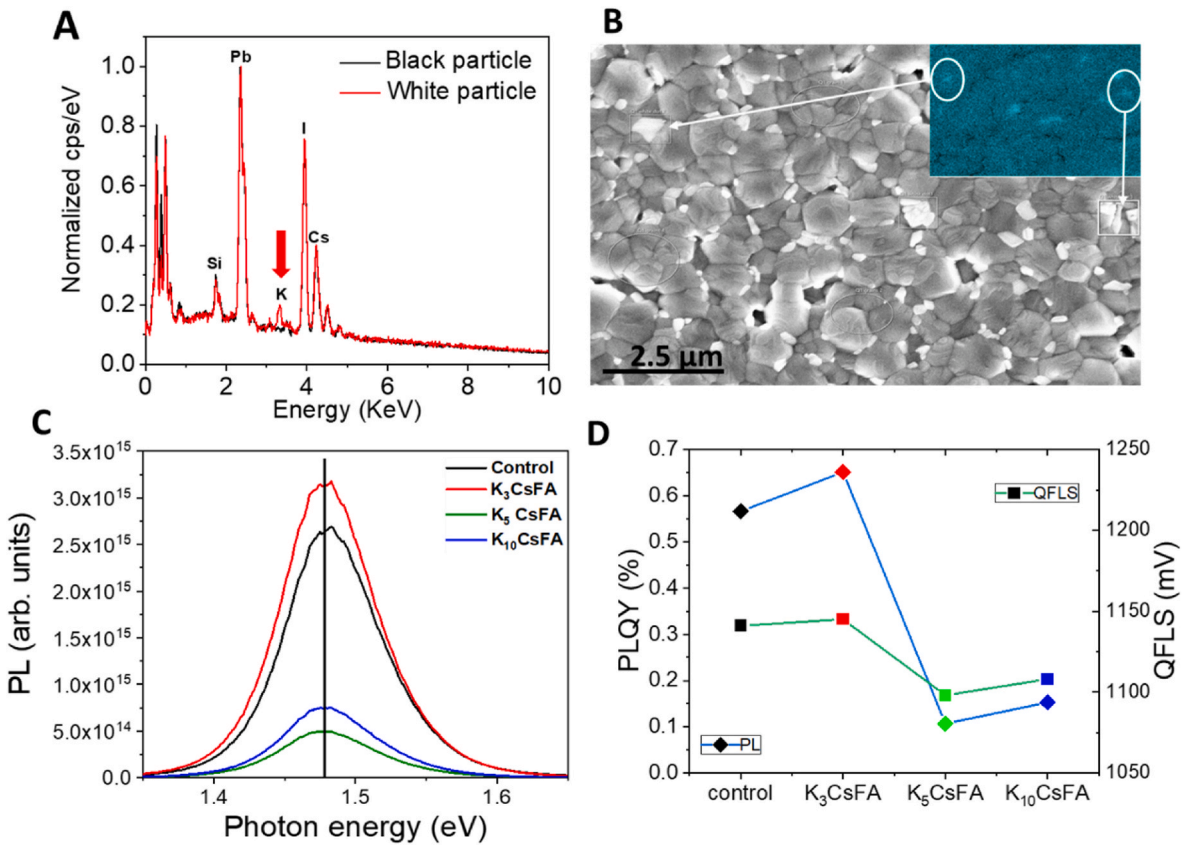

Fig. 3. EDX results of potassium-added and Photoluminescence of perovskite films **A.** EDX mapping of a white particle with excess of potassium and black particle with low content of potassium. **B**. SEM top view image of potassium-based perovskite film, showing the withe and black particle. **C**. Photoluminescence spectra for pristine perovskite films deposited on quartz with no adjacent charge selective contacts, **D**. PL quantum yield (PLQY), and quasi-Fermi level splitting (QFLS) characterizations extracted from absolute PL measurement given in A.

from previous results. Optical properties were studied through photoluminescence (PL) emission, photoluminescence quantum yield (PLQY), and quasi-fermi level splitting characterization (QFLS). The perovskite precursor solution was deposited on glass without hole or electron transport layers to show no interference or contribution from another material. It can be observed from Fig. 3C an increase in the PL emission intensity after the addition of 3% K^+, this enhancement is associated with a non-radiative recombination process reduction, primarily due to defects passivation. In previous results it has been reported that PbI_2 originates recombination centers in the perovskite films, triggering detrimental effects in photoluminescence properties. Hence the enhanced PL emission in 3% K^+ has strengthened our hypothesis that at this level, K^+ is suppressing the diffusion of PbI_2 into the film diminishing non-radiative recombination.

When K^+ concentration was further increased to 5% and 10%, a dramatical PL quenching was observed, even though these films exhibit larger grains and therefore, grain boundaries reduction, as we have seen in SEM images. This apparent lack of correlation can be justified; if at this stage the higher amount of PbI–K compound is originating deep traps at grain boundaries and surface, accelerating carrier losses. We propose that for 5%, 10% and higher concentration of K^+ the surface trap states are the predominant pathways that contribute to non-radiative recombination losses, due to the excess of metallic-like compound at the surface (Fig. S3) and K–PbI molecules passivating the perovskite near the surface. This mechanism is squematically described in the Fig. S4. Nevertheless, broad research is needed to estimate the different defect contributions in the recombination process. It is well known that the presence of non-radiative losses in the absorbent layer limits the performance of solar cells [26]; PLQY quantifies the ratio between radiative and total recombination, values of PLQY closer to the unity are required for radiative recombination. As shown in Fig. 3D and % K^+ exhibits the highest value of PLQY, which implies this concentration shows the lower non-radiative recombination rate, compared to the other concentrations. Meanwhile the quasi-Fermi level splitting (QFLS) (Fig. 3D) for this concentration is 1.14 V, this value is the higher achievable open-circuit voltage that can be reached and was calculated from PLQY (SI), but V_{oc} in perovskite solar cell is always lower due to nonradiative losses phenomena, e.g., non-radiative recombination in bulk and at interfaces, parasitic absorption and disparities in energy alignments at perovskite/charge extraction interfaces [27].

Fig. S5, shows the films absorbance spectra. The control film exhibited the highest absorption, decreasing proportionally as the K^+ content is increased from 3% to 5%. It is noteworthy that the differences among control, 3%, and 5% films are negligible. However, at 10% K^+ film, we can observe a more significant decrease in intensity. As shown in Fig. S6, the perovskite layer thickness has an increment with the addition of K^+, then the reduction in absorption could be associated with this increment and with a detrimental film quality or a less tightly covered surface observed promoted by the presence of high content of K–PbI (brighter domains). Table S2 shows the differences thickness on the different amount of K, the material with 3% of K have 660 nm (see Fig. 4C).

To study the K^+ impact on the device performance, perovskite films were prepared with identical concentrations as previously mentioned and incorporated into a solar cell with tin oxide (SnO_2) and Spiro-OMeTAD as ETM and HTM, respectively. The device architecture and the corresponding complete device cross-sectional SEM images are shown in Fig. 4B and C, respectively.

The perovskite solar cells photovoltaic performance was measured under 1 sun illumination condition (as it is described in supplementary

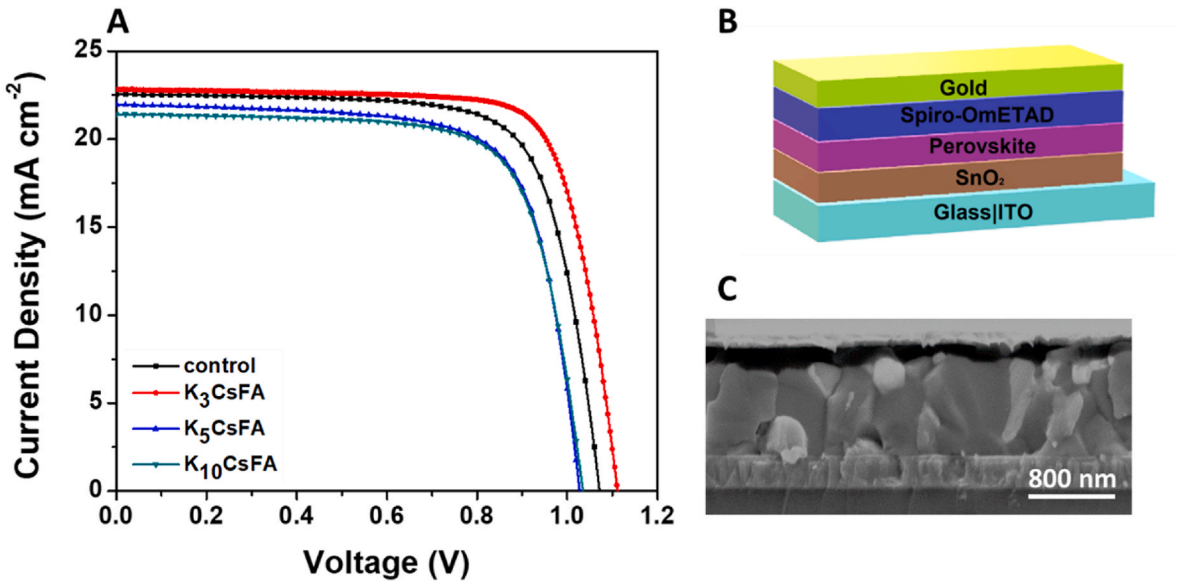

Fig. 4. A. Current density–voltage (*J–V*) curves of champion solar cells for each concentration. **B.** Schematic image of the planar solar cell. **C.** Cross-sectional SEM of a planar perovskite solar cell ITO/SnO_x/perovskite/spiro-MeOTAD/gold with 3% of K^+. (For interpretation of the references to colour in this figure legend, the reader is referred to the Web version of this article.)

information). Fig. 4A show K_xCsFA series presenting the champion devices J-V scans, the corresponding photovoltaic parameters for each concentration are displayed in Table 1. The statistics performance of the planar perovskite solar cells is shown in Fig. 5.

The best photovoltaic performance was obtained from 3% K^+ based devices, achieving a PCE of 19.39% for the champion solar cell. The short-circuit current (J_{sc}) and open-circuit voltage (V_{OC}) values show a significative enhancement after the alkali metal addition. As was mentioned previously small amount of K^+ promotes mitigation of non-radiative recombination pathways and improves crystallinity, thus the JV results show that J_{sc} and V_{OC} evolves accordingly to the film properties. Additionally, detrimental effects in photovoltaic parameters were observed for higher K^+ devices. The control solar cells showed the best FF values among the four concentrations, with a mean value of 73.6%. The FF exhibited a gradually decrease for 3%, 5% and 10% K^+ devices; this was possibly due to PbI_2 accumulation at the surface, hindering charge extraction between perovskite and charge transport layers, inducing a minimized PCE of 16% for 10% K^+ solar cells.

Table 1
Photovoltaic parameters for champion devices and mean values for each concentration.

Sample		J_{sc} (mA cm^{-2})	Integrated J_{sc} (mA cm^{-2})	V_{oc} (V)	FF (%)	PCE (%)
Control	Champion	22.6	22.7	1.07	73.6	17.8
	mean ±	21.75		1.03	73.6	16.45
	SD[a]	± 0.1		± 0.007	± 0.3	± 0.2
K_3CsFA	Champion	22.8	23.6	1.11	76.4	19.39
	mean ±	22.4 ±		1.04	72.8	17.2
	SD[a]	0.09		± 0.006	± 0.3	± 0.1
K_5CsFA	Champion	22.5	21.2	1.03	71.5	16.5
	mean ±	21.5 ±		0.97	69.65	14.85
	SD[a]	0.1		± 0.007	± 0.4	± 0.2
K_{10}CsFA	Champion	21.4	20.0	1.03	72.8	16.1
	mean ±	21.9 ±		1.02	68.7	15.75
	SD[a]	0.1		± 0.006	± 0.8	± 0.2

[a] The mean values are calculated from a batch of 20 devices each.

Additionally, the photostability test of the PSCs was conducted with constant illumination with an adjusted light intensity of 100 mW cm^{-2} at room temperature. In Fig. S8A we can see the stability measure of the best pixel for each devices, where the PSCs with high concentration of K^+ (K_{10}CsFA) rapidly lost more than 80% of their initial PCE (15%) after 7000 s of maximum power point tracking (MPPT), on the other hand, the PSCs with 3% of K^+ (K_3CsFA) exhibit excellent higher stability and retain 80% of the initial efficiency (17%) after 7000 s of continuous MPPT, comparing also with the control devices gradually decrease until they reach 70% of the initial PCE (15%) after 7000 s followed by devices with 5% K^+ addition (K_5CsFA) retained 40% of the initial PCE (16%), also in Fig. S8B we can see the average values form different pixel from each K content, where the composition of K_3CsFA shows better stability losing only 20% in comparison to the others and the improvement in device stability with 3% K^+ addition can be attributed to the enlarged grain size and facilitated charge separation, reducing carrier accumulation at interfaces.

Additionally, the devices external quantum efficiency (EQE) curves at different K^+ concentration were measured (Fig. S7). As is usually reported in EQE characterization for solar cells, the spectra can be subdivided in three distinct regions: for short wavelengths all EQE curves show an edge, this is related to front reflection and parasitic absorption due to ITO and the ETL. Between 450 and 650 nm, EQE reaches the highest values, with a sighting increment at 3% K^+ compared to control device, this increase, evidences the K^+ role as passivating agent, increasing the probability of charge collection due to a lower recombination rate. The devices show a slightly weaker signal over 650 nm, where an EQE decrement in this region is related to a charge extraction reduction at perovskite/HTL interface mainly due to surface recombination, this is consistent with our assumption that K–PbI accumulation at the perovskite surface triggers a detrimental effect creating recombination pathways at perovskite/spiro interface. This effect can be observed more clearly for 5% K^+ and 10% K^+ devices, where the EQE values for wavelengths above 650 nm are noticeable lower. The integrated J_{sc} of the best devices from external quantum efficiency measurement (EQE) integration is shown in Fig. S7 and Table 1.

To investigate in detail the effect of incorporating K^+ during the solar cell operation, we have measured impedance spectroscopy (IS). Fig. 6A shows the impedance spectra for different K_x configurations, measured around V_{oc}. Usually, these spectra are analyzed with an equivalent

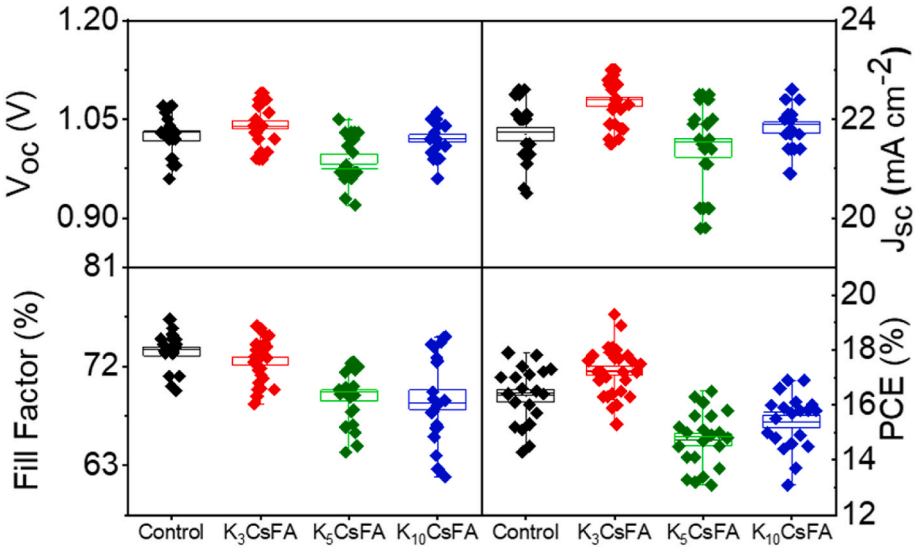

Fig. 5. Statistic of photovoltaic parameters for 20 solar cells for each concentration. The data have been collected over ten different batches.

circuit (EC), allowing the extraction of quantitative parameters. However, the election of this EC is particularly complicated for perovskite solar cells because many have been proposed in the literature. Different ECs were needed to explain different IS responses, including inductive loops [28], negative capacitances [29,30], and diffusion-like arcs [31]. On the other hand, different ECs reproduce the same impedance response, which requires complementary techniques to differentiate them [32,33]. The spectra in Fig. 6A present only two arcs, which is the most typical response for perovskite solar cells. We selected the EC in Fig. 6B because it generates two arcs and has been widely implemented for perovskite solar cells [33,34]. R_s is the series resistance corresponding to the high-frequency limit in this EC. The high-frequency arc is generated by R_{tr} and C_g, mainly associated with transport resistance and the geometrical capacitance of the perovskite device. Finally, the low-frequency arc is generated by R_{rec} and C_{int}, associated with the recombination resistance and an internal capacitance. The parameters obtained from the spectra fitting in Fig. 6A with the EC in Fig. 6B are shown in Table S1.

Fig. 6C shows the characteristic recombination time (τ_{rec}=R_{rec}·C_{int}) compared with the V_{oc} for the devices with different K concentrations. The fact that the V_{oc} follows the response of τ_{rec} implies that it is related to non-radiative recombination kinetics. When τ_{rec} increase means that non-radiative recombination process is slower, which allows a higher charges accumulation and a consequent increment in the V_{oc}. The V_{oc} obtained for these samples have a similar trend to the corresponding samples in Figs. 3 and 5, showing an increase for 3% K^+ compared with the control a pronounced decrease for high K^+ concentrations. Note in Fig. 6E that it is C_{int}, rather than R_{rec}, the parameter that provides the characteristic shape observed for t_{rec}, suggesting a larger charge accumulation which is determining to the higher displacement in Fermi level and thus larger V_{oc}, the same trend as the one found in chemical capacitances [35].

In Fig. 6D each device resistances obtained fitted with the equivalent circuit (Fig. 6B) is shown. The R_s is approximately constant, which is expected because the same contacts were used for all samples. Interestingly, R_{rec} is also approximately constant, which is associated with all measurements being taken at V_{oc}. As observed, the high-frequency arc, given by R_{tr}, mainly dominates the total resistance (R_{tot}=$R_s + R_{tr} + R_{rec}$). This transfer resistance combines transport resistance at the perovskite layer, charge transfer at perovskite interfaces, and high-frequency contribution to recombination resistance [36]. As seen in Fig. 6D, R_{tr} increases with the K incorporation. The simultaneous drop in FF observed in Fig. 6F, suggest that the serial resistance contribution to R_{tr} (transport and charge transfer at contacts) dominate over recombination contributions. We may associate this change either to surface passivation with increased K^+ amount or to a reduction in the charges mobility at the perovskite layer, in this case both effects combination may not be discarded. At 3% K^+, the R_{tr} increase is small, and so is the decrease in FF. At 5% K^+ R_{tr} peaks and FF makes a minimum. The 10% slight change could be due to the growth of the metallic-like grains observed in the SEM images. The differences observed in the geometrical capacitance (C_g) follow the opposite behavior of R_{tr}. Combined with the SEM results, suggesting that the K incorporation increases film thickness, and thus C_g should decrease and R_{tr} increase in the perovskite composition.

3. Conclusions

In summary, we have investigated the effects of KI adding into the perovskite precursor solution on the properties of $CsFAPbI_3$ films and its impact on the photovoltaic performance. We conclude that the incorporation of potassium ion strongly influences the crystallization process and induces the growth of larger grains on the films, this through the uptake of PbI_2 byproduct out the perovskite structure. In short, we conclude that, from our findings we propose a twofold impact of K^+ addition on $CsFAPbI_3$ film, the first one at 3%, K^+ prevents the byproduct deposition on the bulk, and the corresponding uptake near the film surface. But for a higher K^+ concentration, not only contributes to this uptake, the relative excess of this ion start to passivate the perovskite grains surface, this passivation and the bulk-trapped $KPbI_4$ molecules induce a lattice expansion, that is clearly observed on the diffraction peaks shift to lower angles. We found that 3% concentration of K^+ reduces the non-radiative recombination on the film, inducing high values of J_{sc} and V_{oc} for devices fabricated with this concentration. Impedance measurement further confirms our results, from the typical two arc model we observed that τ_{rec} presented the highest value for the 3% K^+ device due to the reduction of non-radiative recombination, matching with V_{oc} and QFLS measurement. Thus, the K^+ incorporation improves significatively the performance of perovskite solar cells, showing a PCE increment of 17.7% for the control device to 19.39% for the 3% K^+ concentration with better stability in a constant measurement. This paper highlights the suitability of K addition into $CsFAPbI_3$ perovskite as a technique to tune the film morphology and optical properties, modulating the solar cell performance simultaneously.

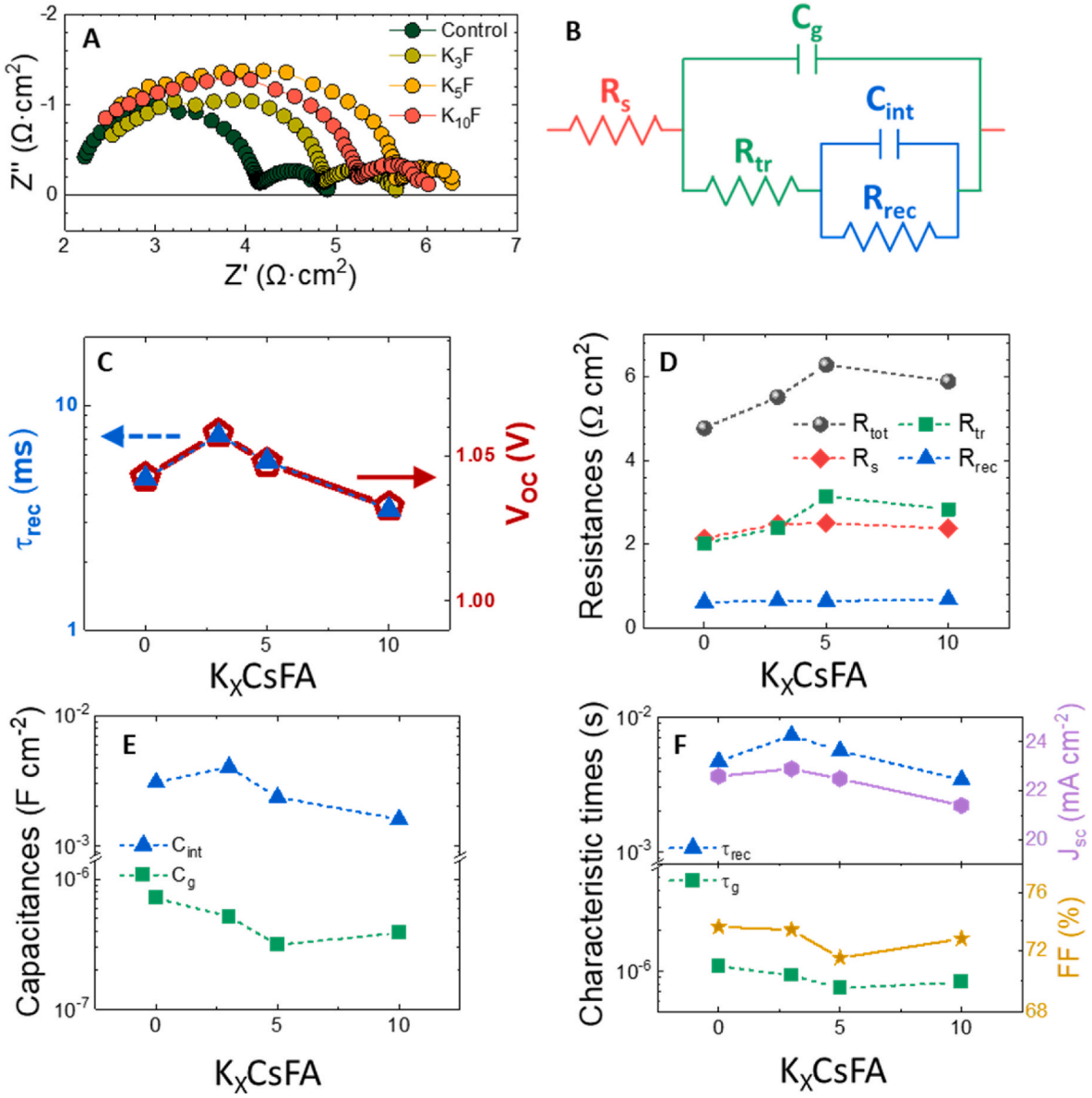

Fig. 6. **A.** Impedance Spectroscopy responses for the different concentrations of K^+, measured around V_{oc}. **B.** Equivalent circuit used to fit these responses, with R_s: series resistance, C_g: geometrical capacitance, R_{tr}: transfer resistance, R_{rec}: recombination resistance and C_{int}: internal capacitance. **C.** Compare the characteristic recombination time (τ_{rec}=R_{rec}·C_{int}) with the V_{oc}, for the different concentrations. **D.** Shows the evolution of the resistances in the equivalent circuit, together with the total resistance (R_{tot}= R_s + R_{tr} + R_{rec}), as a function of the K^+ concentration, **E.** Capacitance data obtained from the fitting and **F.** characteristic times, J_{sc} and FF vs K concentration.

CRediT authorship contribution statement

Gabriela S. Anaya Gonzalez: Investigation, Writing – original draft. **Jose J. Jeronimo-Rendon:** Investigation, Writing – review & editing. **Qiong Wang:** Investigation, Conceptualization. **Guixiang Li:** Investigation. **Agustin O. Alvarez:** Methodology, Investigation. **Francisco Fabregat-Santiago:** Methodology, Conceptualization. **Hans Köbler:** Investigation. **Alberto Alvarado:** Conceptualization. **Hector Juárez-Santiesteban:** Conceptualization. **Silver-Hamill Turren-Cruz:** Investigation, Conceptualization, Writing – review & editing. **Michael Saliba:** Investigation, Conceptualization. **Antonio Abate:** Investigation, Conceptualization, Funding acquisition.

Declaration of competing interest

The authors declare the following financial interests/personal relationships which may be considered as potential competing interests:

Gabriela S. Anaya Gonzalez reports financial support was provided by Consejo Nacional de Ciencia y Tecnología (CONACYT). M. Saliba reports financial support was provided by Helmholtz-Zentrum Berlin for materials and energy. M. Saliba reports financial support was provided by German Research Foundation (DFG). Francisco Fabregat-Santiago, Agustin O. Alvarez reports financial support was provided by Ministerio de Economía y Competitividad (MINECO).

Data availability

Data will be made available on request.

Acknowledgements

Gabriela S. Anaya Gonzalez thanks the Consejo Nacional de Ciencia y

Tecnología (CONACYT) for financial support and The Helmholtz-Zentrum Berlin for materials and energy. M. Saliba received funding from the Helmholtz Young Investigator Program at Forschungszentrum Jülich, Germany. M. Saliba acknowledge funding from the German Research Foundation (DFG), SPP2196 and GRK 2642. A.O.A and S.F.F acknowledge funding from the European Union's Horizon 2020 MSCA Innovative Training Network under grant agreement No 764787, from the Ministerio de Economía y Competitividad (MINECO) of Spain under the project ENE2017-85087-C3-1-R and from the Generalitat Valenciana under the project PROMETEO/2020/028. S.H.T.C would like to thank the Spanish Ministry of Economy, Industry and Competitiveness (post-doctoral contract Juan de la Cierva Formación FJC2019-041835-I) for the financial support during this work.

Appendix A. Supplementary data

Supplementary data to this article can be found online at https://doi.org/10.1016/j.solmat.2022.111964.

References

[1] X.-X. Gao, W. Luo, Y. Zhang, R. Hu, B. Zhang, A. Züttel, et al., Stable and high-efficiency methylammonium-free perovskite solar cells, Adv MPhys chem chem phys PCCPater (Deerfield Beach, Fla.) 32 (9) (2020), e1905502.
[2] Best research-cell efficiency chart, Available from: https://www.nrel.gov/pv/cell-efficiency.html.
[3] W.-J. Yin, T. Shi, Y. Yan, Unusual defect physics in CH 3 NH 3 PbI 3 perovskite solar cell absorber, Appl. Phys. Lett. 104 (6) (2014), 63903.
[4] K.X. Steirer, P. Schulz, G. Teeter, V. Stevanovic, M. Yang, K. Zhu, et al., Defect tolerance in methylammonium lead triiodide perovskite, ACS Energy Lett. 1 (2) (2016) 360–366.
[5] B. Hwang, C. Gu, D. Lee, J.-S. Lee, Effect of halide-mixing on the switching behaviors of organic-inorganic hybrid perovskite memory, Sci. Rep. 7 (2017), 43794.
[6] D. Li, S.A. Bretschneider, V.W. Bergmann, I.M. Hermes, J. Mars, A. Klasen, et al., Humidity-induced grain boundaries in MAPbI 3 perovskite films, J. Phys. Chem. C 120 (12) (2016) 6363–6368.
[7] J.-W. Lee, S.-G. Kim, S.-H. Bae, D.-K. Lee, O. Lin, Y. Yang, et al., The interplay between trap density and hysteresis in planar heterojunction perovskite solar cells, Nano Lett. 17 (7) (2017) 4270–4276.
[8] S.J. Lee, S.S. Shin, Y.C. Kim, D. Kim, T.K. Ahn, J.H. Noh, et al., Fabrication of efficient formamidinium tin iodide perovskite solar cells through SnF_2-Pyrazine complex, J. Am. Chem. Soc. 138 (12) (2016) 3974–3977.
[9] S. Lv, S. Pang, Y. Zhou, N.P. Padture, H. Hu, L. Wang, et al., One-step, solution-processed formamidinium lead trihalide (FAPbI(3-x)Cl(x)) for mesoscopic perovskite-polymer solar cells, Physical chemistry chemical physics PCCP 16 (36) (2014) 19206–19211.
[10] J. Xi, Z. Wu, K. Xi, H. Dong, B. Xia, T. Lei, et al., Initiating crystal growth kinetics of α-HC(NH2)2PbI3 for flexible solar cells with long-term stability, Nano Energy 26 (2016) 438–445.
[11] Y. Wang, H. Zhang, T. Zhang, W. Shi, M. Kan, J. Chen, et al., Photostability of MAPbI 3 perovskite solar cells by incorporating black phosphorus, Sol. RRL 3 (9) (2019), 1900197.
[12] Y. Ouyang, Y. Li, P. Zhu, Q. Li, Y. Gao, J. Tong, et al., Photo-oxidative degradation of methylammonium lead iodide perovskite: mechanism and protection, J. Mater. Chem. 7 (5) (2019) 2275–2282.
[13] S.-H. Turren-Cruz, A. Hagfeldt, M. Saliba, Methylammonium-free, high-performance, and stable perovskite solar cells on a planar architecture, Science (New York, N.Y.) 362 (6413) (2018) 449–453.
[14] W. Zhao, Z. Yao, F. Yu, D. Yang, S.F. Liu, Alkali metal doping for improved CH3NH3PbI3 perovskite solar cells, Adv. Sci. 5 (2) (2018), 1700131.
[15] Z. Tang, S. Uchida, T. Bessho, T. Kinoshita, H. Wang, F. Awai, et al., Modulations of various alkali metal cations on organometal halide perovskites and their influence on photovoltaic performance, Nano Energy 45 (2018) 184–192.
[16] Y. Li, J. Duan, H. Yuan, Y. Zhao, B. He, Q. Tang, Lattice modulation of alkali metal cations doped Cs 1− x R x PbBr 3 halides for inorganic perovskite solar cells, Sol. RRL 2 (10) (2018), 1800164.
[17] T. Ling, X. Zou, J. Cheng, Y. Yang, H. Ren, D. Chen, Modulating surface morphology related to crystallization speed of perovskite grain and optical semiconductor and crystallization properties of the absorber layer under controlled doping of potassium ions for solar cells, Materials 11 (9) (2018).
[18] L. Kuai, Y. Wang, Z. Zhang, Y. Yang, Y. Qin, T. Wu, et al., Passivating crystal boundaries with potassium-rich phase in organic halide perovskite, Sol. RRL 3 (5) (2019), 1900053.
[19] F. Zheng, W. Chen, T. Bu, K.P. Ghiggino, F. Huang, Y. Cheng, et al., Triggering the passivation effect of potassium doping in mixed-cation mixed-halide perovskite by light illumination, Adv. Energy Mater. 9 (24) (2019), 1901016.
[20] J. Chang, Z. Lin, H. Zhu, F.H. Isikgor, Q.-H. Xu, C. Zhang, et al., Enhancing the photovoltaic performance of planar heterojunction perovskite solar cells by doping the perovskite layer with alkali metal ions, J. Mater. Chem. 4 (42) (2016) 16546–16552.
[21] D.J. Kubicki, D. Prochowicz, A. Hofstetter, S.M. Zakeeruddin, M. Grätzel, L. Emsley, Phase segregation in potassium-doped lead halide perovskites from 39K solid-state NMR at 21.1 T, J. Am. Chem. Soc. 140 (23) (2018) 7232–7238.
[22] M.I. Saidaminov, K. Williams, M. Wei, A. Johnston, R. Quintero-Bermudez, M. Vafaie, et al., Multi-cation perovskites prevent carrier reflection from grain surfaces, Nat. Mater. 19 (4) (2020) 412–418.
[23] H.X. Dang, K. Wang, M. Ghasemi, M.-C. Tang, M de Bastiani, E. Aydin, et al., Multi-cation synergy suppresses phase segregation in mixed-halide perovskites, Joule 3 (7) (2019) 1746–1764.
[24] W.A. Saidi, J.J. Choi, Nature of the cubic to tetragonal phase transition in methylammonium lead iodide perovskite, J. Chem. Phys. 145 (14) (2016), 144702.
[25] M. Abdi-Jalebi, Z. Andaji-Garmaroudi, S. Cacovich, C. Stavrakas, B. Philippe, J. M. Richter, et al., Maximizing and stabilizing luminescence from halide perovskites with potassium passivation, Nature 555 (7697) (2018) 497–501.
[26] N. Pellet, P. Gao, G. Gregori, T.-Y. Yang, M.K. Nazeeruddin, J. Maier, et al., Mixed-organic-cation perovskite photovoltaics for enhanced solar-light harvesting, Angew. Chem. 126 (12) (2014) 3215–3221.
[27] S. Mahesh, J.M. Ball, R.D.J. Oliver, D.P. McMeekin, P.K. Nayak, M.B. Johnston, et al., Revealing the origin of voltage loss in mixed-halide perovskite solar cells, Energy Environ. Sci. 13 (1) (2020) 258–267.
[28] A. Guerrero, G. Garcia-Belmonte, I. Mora-Sero, J. Bisquert, Y.S. Kang, T. J. Jacobsson, et al., Properties of contact and bulk impedances in hybrid lead halide perovskite solar cells including inductive loop elements, J. Phys. Chem. C 120 (15) (2016) 8023–8032.
[29] E. Ghahremanirad, A. Bou, S. Olyaee, J. Bisquert, Inductive loop in the impedance response of perovskite solar cells explained by surface polarization model, J. Phys. Chem. Lett. 8 (7) (2017) 1402–1406.
[30] A.O. Alvarez, R. Arcas, C.A. Aranda, L. Bethencourt, E. Mas-Marzá, M. Saliba, et al., Negative capacitance and inverted hysteresis: matching features in perovskite solar cells, J. Phys. Chem. Lett. 11 (19) (2020) 8417–8423.
[31] V. Babu, R. Fuentes Pineda, T. Ahmad, A.O. Alvarez, L.A. Castriotta, A. Di Carlo, et al., Improved stability of inverted and flexible perovskite solar cells with carbon electrode, ACS Appl. Energy Mater. 3 (6) (2020) 5126–5134.
[32] A.O. Alvarez, S. Ravishankar, F. Fabregat-Santiago, Combining modulated techniques for the analysis of photosensitive devices, Small Methods 5 (10) (2021), e2100661.
[33] S. Ravishankar, C. Aranda, S. Sanchez, J. Bisquert, M. Saliba, G. Garcia-Belmonte, Perovskite solar cell modeling using light- and voltage-modulated techniques, J. Phys. Chem. C 123 (11) (2019) 6444–6449.
[34] D. Di Girolamo, N. Phung, M. Jošt, A. Al-Ashouri, G. Chistiakova, J. Li, et al., From bulk to surface: sodium treatment reduces recombination at the nickel oxide/perovskite interface, Adv. Mater. Interfac. 6 (17) (2019), 1900789.
[35] J. Bisquert, Chemical capacitance of nanostructured semiconductors: its origin and significance for nanocomposite solar cells, Phys. Chem. Chem. Phys. 5 (24) (2003) 5360.
[36] E.J. Juarez-Perez, R.S. Sanchez, L. Badia, G. Garcia-Belmonte, Y.S. Kang, I. Mora-Sero, et al., Photoinduced giant dielectric constant in lead halide perovskite solar cells, J. Phys. Chem. Lett. 5 (13) (2014) 2390–2394.